IOP Publishing Plasma Sources Science and Technology

Plasma Sources Sci. Technol. **23** (2014) 035011 (7pp) doi:10.1088/0963-0252/23/3/035011

Electron collisions with cesium atoms—benchmark calculations and application to modeling an excimer-pumped alkali laser

Oleg Zatsarinny[1], **Klaus Bartschat**[1,2], **Natalia Yu Babaeva**[3] and **Mark J Kushner**[3]

[1] Department of Physics and Astronomy, Drake University, Des Moines, IA 50311, USA
[2] ITAMP, Harvard-Smithsonian Center for Astrophysics, Cambridge, MA 02138, USA
[3] Electrical Engineering and Computer Science Department, University of Michigan, Ann Arbor, MI 48109, USA

E-mail: oleg.zatsarinny@drake.edu, klaus.bartschat@drake.edu, nbabaeva@umich.edu and mjkush@umich.edu

Received 26 February 2014, revised 1 April 2014
Accepted for publication 2 April 2014
Published 19 May 2014

Abstract

The *B*-spline *R*-matrix (BSR) with pseudostates method is employed to describe electron collisions with cesium atoms. Over 300 states are kept in the close-coupling expansion, including a large number of pseudostates to model the effect of the Rydberg spectrum and, most importantly, the ionization continuum on the results for transitions between the discrete physical states of interest. Predictions for elastic scattering, momentum transfer, excitation and ionization are presented for incident energies up to 200 eV and compared with results from previous calculations and available experimental data. In a second step, the results are used to model plasma formation in an excimer-pumped alkali laser operating on the Cs ($6^2P_{3/2,1/2} \rightarrow 6^2S_{1/2}$) (852 nm and 894 nm) transitions. At sufficiently high operating temperature of a Cs–Ar containing quartz cell, pump power, and repetition rate, plasma formation in excess of 10^{14}–10^{15} cm^{-3} occurs. This may reduce laser output power by electron collisional mixing of the upper and lower laser levels.

Keywords: electron–cesium collisions, cross section, elastic scattering, excitation, ionization, momentum transfer, excimer-pumped alkali laser

(Some figures may appear in colour only in the online journal)

1. Introduction

As noted in our previous paper on the subject [1], electron scattering from Cs has received significant attention, both experimentally [2–9] and theoretically [10–20]. Being a heavy target with nuclear charge $Z = 55$, relativistic effects are expected to be important. On the other hand, being an alkali atom, it is likely that many aspects of the collision can be modeled well as a quasi-two-electron problem, especially for energies below the threshold for excitation and ionization of inner shells. Hence, much effort has been devoted to developing suitable model potentials to account for the interaction of the projectile with the valence electron and of both with the core. To mention just one example, adding a small dielectronic term [12] to the core potential obtained by optimizing the Rydberg spectrum proved to be the critical ingredient for moving the $(6s6p)^3P_{0,1,2}$ negative-ion configuration from previously predicted bound states to very low-energy (a few meV) resonances in the elastic channel, a prediction that was ultimately confirmed experimentally [21].

Apart from its role as a suitable target to study fundamental collision physics, in particular as a testing ground for state-of-

the-art scattering theory, Cs is also of practical importance in many applied areas. One example is an excimer-pumped alkali laser (XPAL), where lasing on the Cs $(6p)^2P_{1/2} \rightarrow (6s)^2S_{1/2}$ transition at 852 nm occurs when pumping on the blue satellite of the Cs $(6s)^2S_{1/2} \rightarrow (6p)^2P_{3/2}$ transition, peaking at 837 nm for mixtures of Cs vapor and Ar [22–24]. The intermediate state is the alkali-rare gas excimer CsAr ($B\,^2\Sigma^+_{1/2}$).

A potentially important issue in high power pumping of XPAL is the formation of plasma by electrons that are superelastically heated by collisions with the resonant states of Cs. This is a process analogous to LIBORS (laser ionization by optical resonance saturation), whereby alkali atoms may be nearly fully ionized by laser excitation of the resonance states [25]. The analysis and modeling of XPAL systems based on Cs have been challenged by the lack of a comprehensive set of electron impact cross sections for Cs [26]. The utility of the Cs cross sections reported here will be demonstrated by analysis of the Cs/Ar XPAL system and the prediction of plasma formation under high power pumping.

This paper is organized as follows. In section 2 we briefly describe our numerical method to treat e–Cs collisions. This is followed in section 3 by the presentation and discussion of our predicted elastic, momentum-transfer, excitation, ionization and total cross sections, where the initial state can be either the $(6s)^2S_{1/2}$ ground state or one of the excited $(6p)^2P_{1/2,3/2}$ states. The modeling is discussed in section 4, and we finish with a brief summary (section 5).

2. Theoretical approach

The calculations performed for this work are based on two independent *ab initio* *R*-matrix (close-coupling) models. The first one is a semi-relativistic approach, in which relativistic effects for the valence and the projectile electrons were accounted for through the one-electron terms of the Breit–Pauli Hamiltonian. This BPRM model is an extension of the work described by Bartschat and Fang [17] to incident energies up to 50 eV. Depending on the incident energy, between 5 and 40 states (including pseudostates to account for the possibility of ionization) were retained in the close-coupling expansion of the quasi-two-electron scattering system. By carefully analyzing the results from the various models, we chose what we believe is the 'best set' of our BPRM predictions.

The principal purpose of the Breit–Pauli calculations, however, was to present an independent check for the full-relativistic model described below. One would generally expect that accounting for relativistic effects at the Breit–Pauli level is sufficiently accurate for low-energy e–Cs scattering involving only the valence electron. This expectation was confirmed in [14], where more details can be found. The effect of the core electrons in the BP model was described by a local model potential, which was optimized to generate a highly accurate valence electron spectrum for neutral Cs, as well as the electron affinity of Cs^- by adding the dielectronic term suggested in [12]. As a result, it is likely that the very low-energy regime (below about 0.1 eV) is described very well by this model.

The second approach is a fully relativistic, all-electron *B*-spline *R*-matrix with pseudostates (DBSR) ansatz. This model is a significant extension of the work described by Zatsarinny and Bartschat [1]. In the latter, most results were obtained in a 12-state model, including the $(6s)^2S_{1/2}$ ground state and the physical excited states $(6p)^2P_{1/2,3/2}$, $(5d)^2D_{3/2,5/2}$, and $(7s)^2S_{1/2}$ states, respectively. Another six pseudostates were then selected, since they had a fairly significant dipole connection to the ground state. Some larger models, including one with 20 physical bound states up to $(5f)^2F_{5/2,7/2}$ and one with another 10 pseudostates, were also set up. However, the effect of these additional states was only tested for a few partial waves, due to the large computational effort required and the limited resources available at the time.

In this work, the 30-state model (labeled DBSR-30 below) was run to convergence with respect to the number of partial waves (up to total electronic angular momentum $J = 45$ for the projectile–target system), and a much larger model, coupling a total of 311 states, was set up and also pushed to convergence. This DBSR-311 approach is not only expected to handle ionization via reinterpretation of the results for excitation of pseudostates above the ionization threshold, but it should also provide a very good indication about the likely convergence of the results for transitions between the low-lying physical states with respect to the number of states retained in the close-coupling expansion. In contrast to electron collisions with noble gases, where this convergence can be very slow [27, 28], one generally expects a much faster convergence for alkali targets, especially for transitions from the ground state. Nevertheless, it is important to check this expectation, especially for transitions from already excited initial states. In high density plasmas (see below) such transitions can be important, since there is a good chance of further electron-induced excitation, de-excitation or ionization before the excited atom relaxes back to the ground state by optical decay.

As mentioned above, relativistic effects in the DBSR calculations were accounted for at the level of the Dirac–Coulomb Hamiltonian, exchange effects between all electrons were treated with properly antisymmetrized wavefunctions, and the most important core polarization effects were accounted for by opening up the $5s^2$ and $5p^6$ subshells. For low-energy elastic scattering below the first excitation threshold, where polarization effects are most critical, a special polarized pseudostate model was developed in order to reproduce the static dipole polarizability of the Cs ground state with an accuracy matching the best currently available experimental data. Many more details about the BSR approach can be found in [29] and a recent Topical Review [30].

3. Results for angle-integrated cross sections

Figure 1 shows the angle-integrated elastic cross section for electron collisions with Cs atoms in their $(6s)^2S_{1/2}$ ground state as a function of the collision energy. There is good agreement between the DBSR-311 and the BPRM results, except for energies below 0.1 eV. Here the DBSR-311 model predicts a resonance maximum in the p-wave, but in contrast

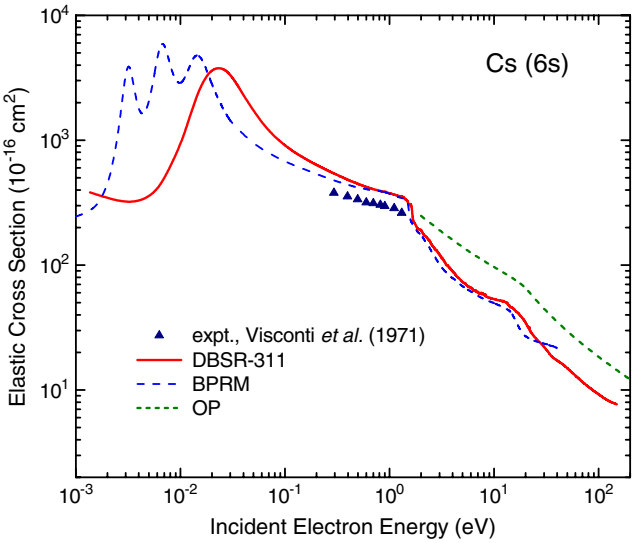

Figure 1. Angle-integrated elastic cross section for electron collisions with Cs atoms in their $(6s)^2S_{1/2}$ ground state. The full-relativistic DBSR-311 results are compared with the predictions from the semi-relativistic BPRM model, the optical potential (OP) approach [20], and the experimental data of Visconti *et al* [3]. For elastic scattering, the DBSR-30 results are very close to those from the DBSR-311 model and hence not shown for clarity of the figure.

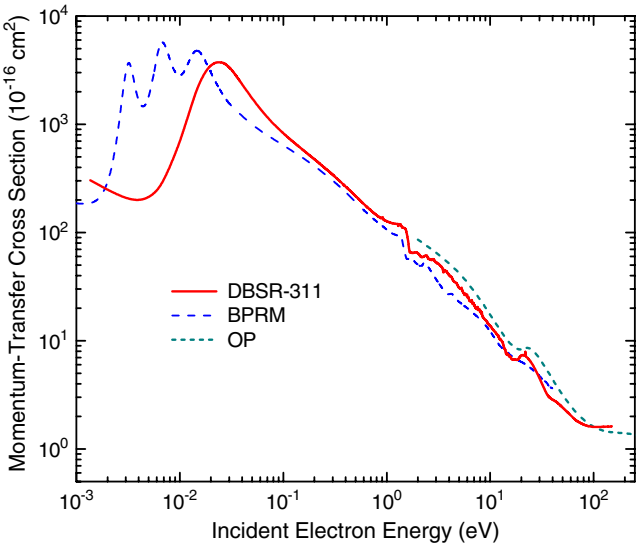

Figure 2. Same as figure 1, except that there are no experimental data available.

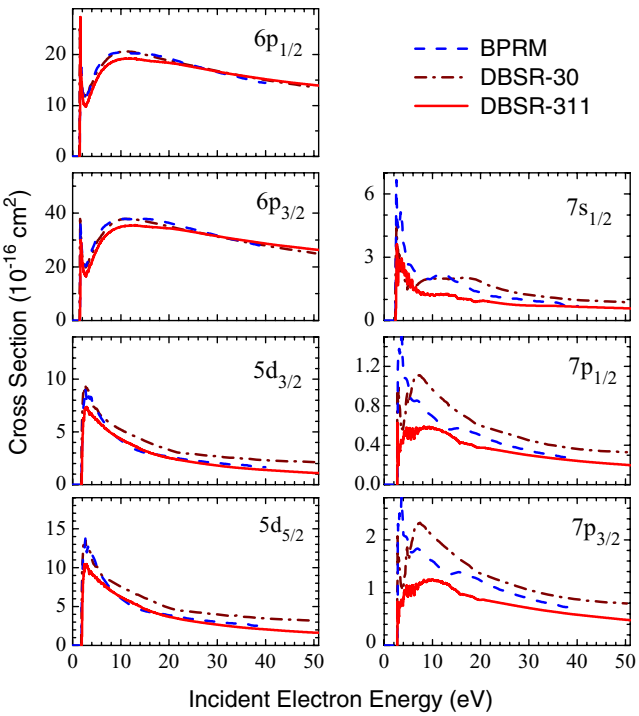

Figure 3. Angle-integrated cross section for electron-impact excitation of the $(6p)^2P_{1/2,3/2}$, $(5d)^2D_{3/2,5/2}$, $(7s)^2S_{1/2}$ and $(7p)^2P_{1/2,3/2}$ states in Cs atoms from the $(6s)^2S_{1/2}$ ground state. The full-relativistic DBSR-30 and DBSR-311 results are compared with the predictions from the semi-relativistic BPRM model.

to the BPRM model [14] (and also the 5-state full-relativistic calculation of Thumm and Norcross [12]), the $(6s6p)^3P_{0,1,2}$ fine-structure components of this feature overlap and hence the fine-structure is not resolved. The position of this maximum is also somewhat high compared with experiment [21]. This demonstrates the difficulty to obtain such a fine detail in a fully *ab initio* model, without any assistance from experiment (in this case structure information), which is included in the phenomenological core potential. As found in many other calculations as well, the experimental data of Visconti *et al* [3] (available in the 0.3–2 eV range), lie below the theoretical predictions. Finally, the 'optical potential' (OP) results of Gangwar *et al* [20] are significantly (up to a factor 2) larger than both our BPRM and DBSR-311 results.

The corresponding predictions for the momentum-transfer cross section are shown in figure 2. The general features are the same as for the elastic cross section shown in figure 1, except that the OP results are significantly closer to those obtained with BPRM and DBSR-311. No experimental data are available for this case.

Figure 3 depicts results for excitation from the $(6s)^2S_{1/2}$ ground state. In particular, for the strong optically allowed $(6s)^2S_{1/2} \rightarrow (6p)^2P_{1/2,3/2}$ resonance transitions, the convergence is excellent with the number of coupled states included in the close-coupling expansion. This is a well-known feature of electron-alkali scattering, where the large oscillator strength of these transitions not only leads to large cross sections, but also accounts for about 99% of the dipole polarizability of the ground state. For the other transitions, the convergence is still encouraging, with the smaller models generally overestimating what we believe is the actual cross section. Not surprisingly, the reduction effect due to additional channel-coupling is most visible for the smallest cross sections, in this case those for excitation of the $(7p)^2P_{1/2,3/2}$ states.

Predictions for excitation from the $(6p)^2P_{1/2}$ and $(6p)^2P_{3/2}$ excited states are presented in figure 4. Again, the agreement between the DBSR-30 and DBSR-311 predictions is generally good, while larger deviations are noticeable compared with some of the BPRM results. We have no explanation for the latter observation, but we do believe that the DBSR-311 data represent the most reliable set and should be used in modeling applications.

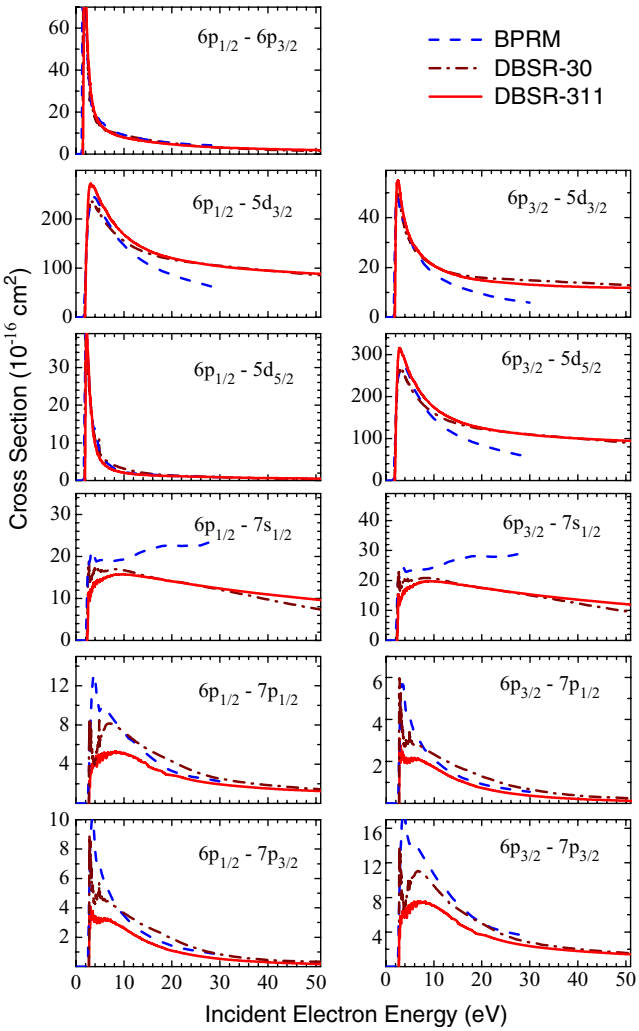

Figure 4. Same as figure 3 for transitions from the $(6p)^2P_{1/2}$ and $(6p)^2P_{3/2}$ excited states.

Results for electron-impact ionization of ground-state Cs atoms are exhibited in figure 5. In the energy region where only the 6s electron can be ionized, there is reasonably good agreement between the BPRM and DBSR-311 predictions, as well as the non-relativistic convergent close-coupling (CCC) results [8]. The DBSR-311 model even reproduces, at least qualitatively, the structure seen experimentally [2] around 15 eV incident energy, which is due to significant excitation of a wealth of autoionizing $5p^5n_1\ell_1n_2\ell_2$ states [31]. Since obtaining the branching ratios for autoionization versus optical decay of these autoionizing states is very complex, we have assumed a 100% contribution to the ionization signal from their excitation. It is, therefore, not surprising that the calculation is slightly overestimating the ionization cross section for incident energies in the 12–20 eV range.

The energy dependence of the cross section data was experimentally determined by Tate and Smith [2]. We normalized their data via a visual fit to the DBSR-311 predictions in the energy region below 20 eV. The absolute values are about 10% lower than the normalization to the CCC results chosen in [8].

Results for ionization from the $(6p)^2P_{3/2}$ excited state are presented in figure 6. Not surprisingly, the agreement between

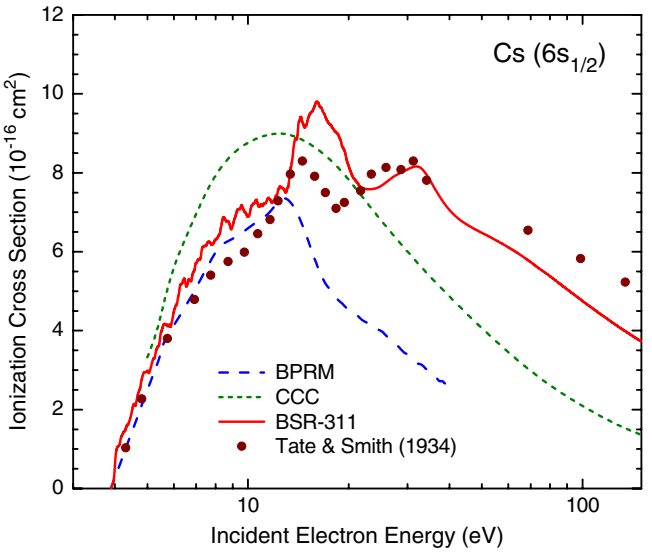

Figure 5. Angle-integrated cross section for electron-impact ionization of Cs atoms in their $(6s)^2S_{1/2}$ ground state. The full-relativistic DBSR-311 results are compared with the predictions from the semi-relativistic BPRM model and non-relativistic convergent close-coupling (CCC) approach. Also shown are experimental data from Tate and Smith [2], which were visually normalized to the DBSR-311 predictions and thus are about 10% lower than the normalization to the CCC results presented by Lukomski *et al* [8]. The ragged structures in the DBSR-311 results at the few-per cent level are due to the finite density of states in the pseudostate spectrum.

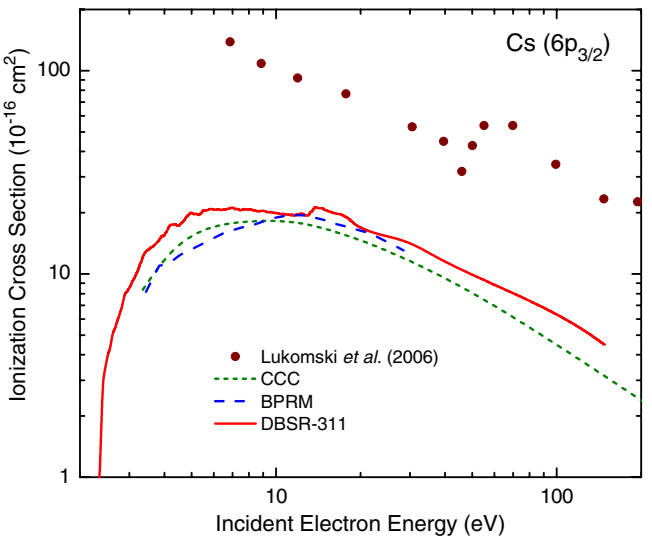

Figure 6. Angle-integrated cross section for electron-impact ionization of Cs atoms in the $(6p)^2P_{3/2}$ excited state. The full-relativistic DBSR-311 results are compared with the predictions from the semi-relativistic BPRM model and the non-relativistic CCC approach. Also shown are the experimental data of Lukomski *et al* [8].

DBSR-311, BPRM, and CCC is very good, and hence the well-known discrepancy of nearly an order of magnitude with the experimental data of Lukomski *et al* [8] persists. We refrain from speculating about possible reasons for this discrepancy, but we are pleased by the agreement among the three theoretical datasets, which were obtained in entirely independent ways.

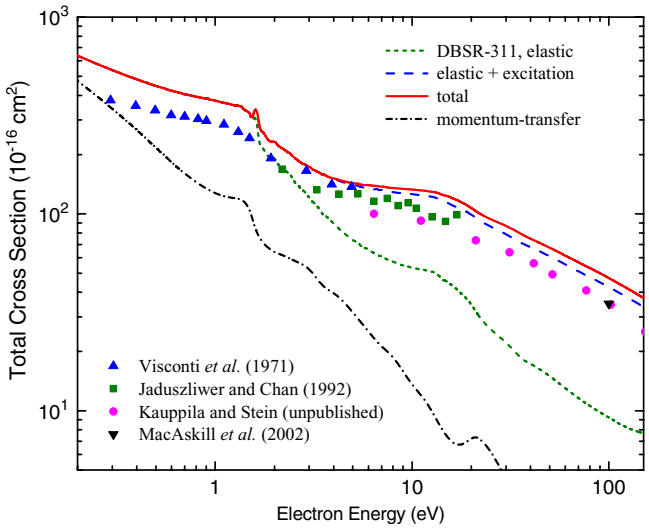

Figure 7. Total electron scattering cross section from the ground $(6s)^2S_{1/2}$ ground state of Cs. The present DBSR-311 results are compared with various sets of experimental data [3, 4, 6, 7]. Also shown are the contributions from elastic scattering as well as elastic scattering plus excitation of discrete states and, finally, the momentum-transfer cross section.

We finish this section with a presentation of the total cross section for electron collisions with Cs atoms in their ground state. The DBSR-311 results are shown in figure 7, where we also include the individual contributions from elastic scattering alone and together with an estimate for excitation of all discrete physical states below the ionization threshold. Note the dominance of excitation over elastic scattering and also ionization, essentially as soon as excitation to the $(6p)^2P_{1/2,3/2}$ is energetically allowed. As mentioned above, this is due to the large oscillator strengths of the resonance transitions and yields a completely different picture when compared with electron collisions with noble gases [27, 28]. For completeness, we also include the momentum-transfer cross section in the figure, in order to compare it directly with the elastic result. Finally, all existing experimental data lie systematically below theory. We have no explanation for this, but we re-emphasize that other calculations [13, 14] have found the same qualitative result.

4. Application to modeling an excimer-pumped laser

In this section, we demonstrate the utility of the Cs electron impact cross sections by their use in a first-principles global model for the Ar/Cs XPAL system. This effort investigated the possible formation of plasma during high repetition rate, high power optical pumping and the consequences on laser performance. In the Cs/Ar XPAL system the CsAr $(B\,^2\Sigma^+_{1/2})$ state is optically pumped by 837 nm pulses. The excimer rapidly dissociates, which produces atoms in the Cs $(6p)^2P_{3/2}$ state. Lasing can then occur on the Cs $(6p)^2P_{3/2} \rightarrow (6s)^2S_{1/2}$ (D_2) transition at 852.1 nm. Plasma can be formed by superelastic heating of sparse seed electrons and by associative ionization of high-lying states of Cs. Once the plasma is formed, stepwise ionization of all excited states of Cs is also an important source of plasma.

The model used in this investigation is `Global_Kin`, a global plasma kinetics model, which is essentially the same as described in [32]. In `Global_Kin`, rate equations for a species densities, temperatures, pump intensities and laser intensities are integrated as a function of time over successive pulsed pump periods. Electron-impact processes are included for elastic and inelastic collisions, accounting for electronic and vibrational excitation, superelastic collisions, ionization and recombination. All rate coefficients for electron-impact processes are functions of electron temperature, T_e, which is determined by solving an electron energy conservation equation. The rate coefficients for electron processes are obtained from solutions of Boltzmann's equation for the electron energy distribution function (EED) using the just described cross sections.

The EEDs and electron impact rate coefficients for an Ar/Cs $= 1/10^{-4}$ mixture for the values of T_e expected during XPAL operation are shown in figure 8. (For these non-Maxwellian distributions, $T_e = (2/3)\langle\varepsilon\rangle$, where $\langle\varepsilon\rangle$ is the average electron energy.) The momentum transfer cross section is in excess of 100 Å^2 at energies below 1.5 eV, and the inelastic threshold for excitation of the Cs $(6p)^2P_{1/2}$ state is 1.38 eV. The end result is that the EED is cut off for electron temperatures $T_e < 0.5$–0.7 eV. At the same time, the low threshold energies and large inelastic cross sections produce significant rate coefficients for electron-impact excitation at moderate T_e. The superelastic rate coefficients, which quench the Cs (6p) states and produce electron heating, have rate coefficients in excess of 10^{-7} cm^3 s^{-1}.

In the demonstration XPAL system, pump radiation propagates through a quartz cell heated to 450 K containing 500 Torr of Ar and Cs vapor (mole fraction 6.85×10^{-5}). The pump pulses at 837 nm are 4 ns (full width half maximum) with a 3 μs inter-pulse period. A sufficient number of pump cycles were calculated to achieve a pulse-periodic steady state in excited state and plasma densities. The electron densities over successive pulses for different maximum pump intensities are shown in figure 9. Plasma is formed by heating of background electrons via superelastic relaxation of dominantly the Cs $(6p)^2P_{3/2,1/2}$ states. A pulse-periodic steady state is reached after 10–60 pump pulses with electron and ion densities of (2–5) $\times 10^{14}$ cm^{-3}.

The densities of states responsible for lasing are also shown in figure 9 for the 1st and 81st pulses for an 8 MW cm^{-2} pump pulse. T_e peaks at 0.4 eV during early pulses of the pumping and 0.7 eV in later pulses, and it decreases during the inter-pulse period to about 0.2 eV. The nearly horizontal dashed line in figure 9 shows the sum of the densities of Cs^+ and Cs_2^+. The density of CsAr $(B\,^2\Sigma^+_{1/2})$ follows the intensity of the pump pulse, as its dissociative lifetime is <1 ns. The laser transition is saturated by a high intra-cavity laser intensity, indicated by the densities of the Cs $(6p)^2P_{3/2}$ and the Cs $(6s)^2S_{1/2}$ states being in the ratio of their degeneracies. The plasma density of 2×10^{14} cm^{-3} on the 81st pulse is predominantly Cs^+ with a small contribution from Cs_2^+. With an initial Cs density of 7×10^{14} cm^{-3}, there is significant ionization of the Cs, which contributes to the depletion of the ground state. The laser pulse length decreases from 15 ns on

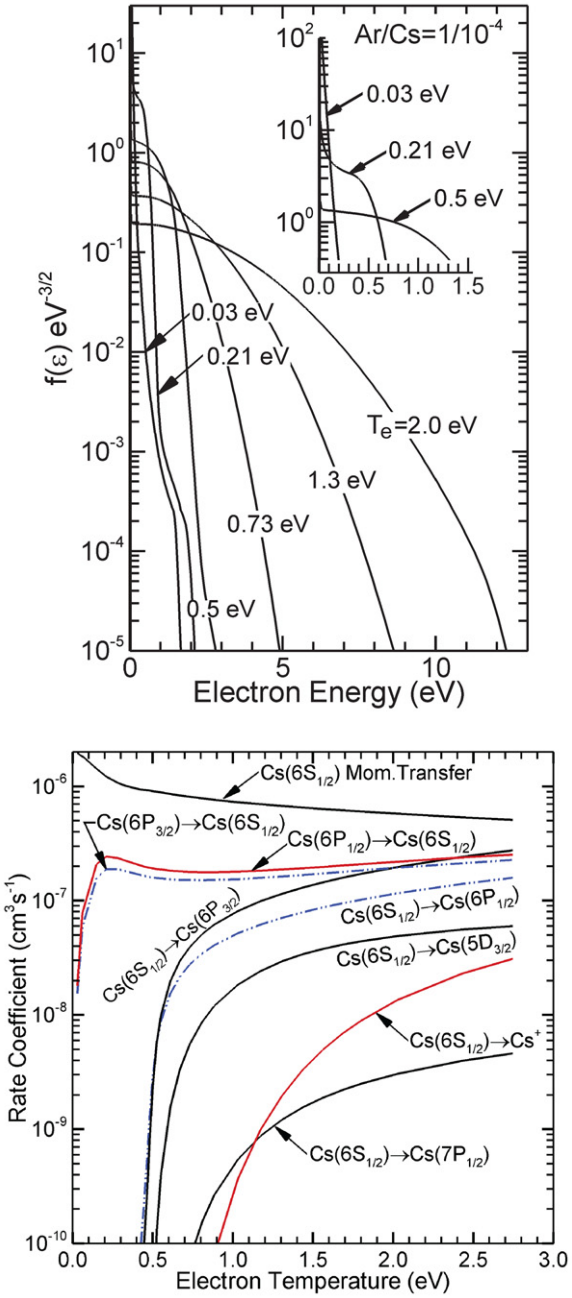

Figure 8. Transport properties of an Ar/Cs = $1/10^{-4}$ plasma. Top: electron energy distributions (EEDs) for different average electron temperatures. The inset shows detail of the EEDs at low electron energy. Bottom: rate coefficients for electron-impact processes as a function of electron temperature (1 eV ≈ 11 600 K).

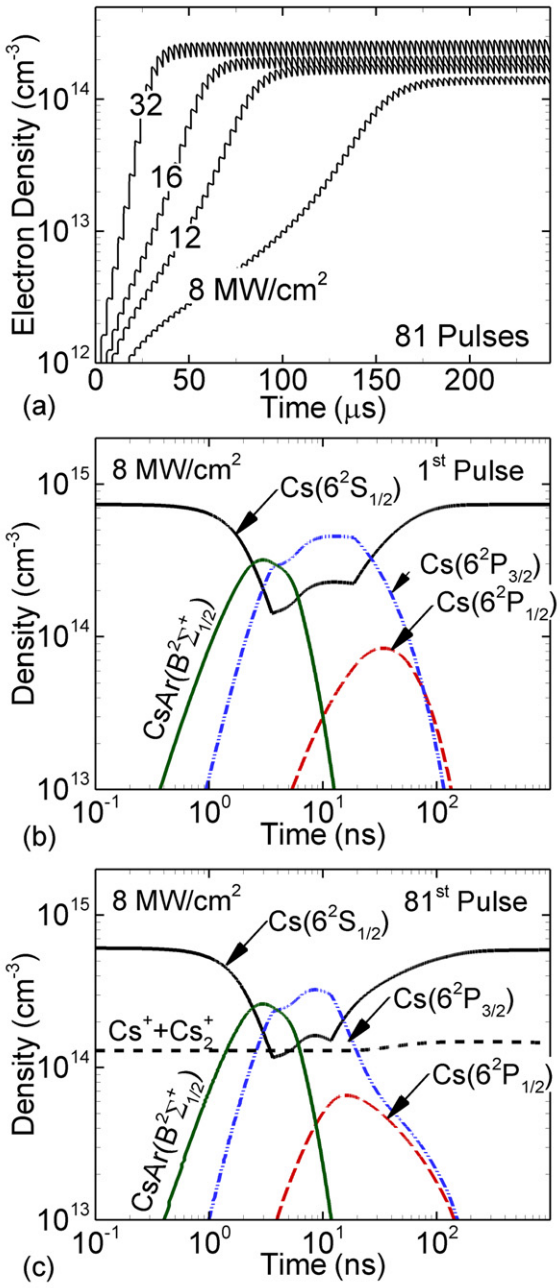

Figure 9. Properties of the XPAL operating on Cs vapor. (*a*) Electron density for high repetition rate optical pumping for different pump intensities. Density of species responsible for lasing (852 nm) during the (*b*) 1st and (*c*) 81st pump pulse.

the first pump pulse to 9 ns on the 81st pump pulse due to the depletion of the ground state by ionization and electron collision mixing of the laser levels.

5. Summary and conclusion

We have presented datasets for electron collision cross sections with Cs atoms initially in either the $(6s)^2S_{1/2}$ ground state or the excited $(6p)^2P_{1/2,3/2}$ states. The present DBSR-311 results, obtained in a full-relativistic close-coupling with pseudostates approach, are a significant extension of previous work, both regarding the number of coupled states, the processes considered and the range of energies covered.

The results were then used to model an excimer-pumped alkali laser with Cs as one of the species. The utility of the electron impact cross section set was demonstrated through global modeling of the Cs/Ar excimer-pumped-alkali laser (XPAL), which oscillates on the Cs $(6p)^2P_{3/2} \rightarrow (6s)^2S_{1/2}$ (D_2) transition at 852.1 nm. Heating of electrons by superelastic relaxation of the excimer excited Cs $(6p)^2P_{3/2,1/2}$ resonant states lead to significant plasma formation, which ultimately reduces laser power by depletion of the ground state

through ionization and by electron collision mixing of the laser levels.

Acknowledgments

This work was supported by the NSF under grants No PHY-1068140, PHY-1212450, and the XSEDE allocation PHY-090031 (OZ, KB), and by the DoD High Energy Laser Multidisciplinary Research Initiative (NYB, MJK).

References

[1] Zatsarinny O and Bartschat K 2008 *Phys. Rev.* A **77** 062701
[2] Tate J T and Smith P T 1934 *Phys. Rev.* **46** 773
[3] Visconti P J, Slevin J A and Rubin K 1970 *Phys. Rev.* A **3** 1310
[4] Jaduszliwer B and Chan Y C 1992 *Phys. Rev.* A **45** 197
[5] Baum G, Raith W, Roth B, Tondera M, Bartschat K, Bray I, Ait-Tahar S, Grant I P and Norrington P H 1999 *Phys. Rev. Lett.* **47** 1128
[6] Stein T S and Kauppila W E 2001 unpublished (cited in [7])
[7] MacAskill J A, Kedzierski W, McConkey J W, Domyslawska J and Bray I 2002 *J. Electron Spectrosc Relat. Phenom.* **123** 173 (and private communication)
[8] Lukomski M, Sutton S, Kedzierski W, Reddish T J, Bartschat K, Bartlett P L, Bray I, Stelbovics A T and McConkey J W 2006 *Phys. Rev.* A **74** 032708
[9] Baum G Pavlovic N, Roth B, Bartschat K, Fang Y and Bray I 2002 *Phys. Rev.* A **66** 022705
[10] Karule E 1972 *J. Phys. B: At. Mol. Opt. Phys.* **5** 2051
[11] Scott N S, Bartschat K, Burke P G, Eissner W B and Nagy O 1984 *J. Phys. B: At. Mol. Opt. Phys.* **17** L191
[12] Thumm U and Norcross D W 1991 *Phys. Rev. Lett.* **67** 3495
[13] Thumm U and Norcross D W 1993 *Phys. Rev.* A **47** 305
[14] Bartschat K 1993 *J. Phys. B: At. Mol. Opt. Phys.* **26** 3595
[15] Bartschat K and Bray I 1996 *Phys. Rev.* A **54** 1723
[16] Ait-Tahar S, Grant I P and Norrington P H 1997 *Phys. Rev. Lett.* **79** 2955
[17] Bartschat K and Fang Y 2000 *Phys. Rev.* A **66** 052719
[18] Ahmed Md F, Ji W, McEachran R P and Stauffer A D 2007 *J. Phys. B: At. Mol. Opt. Phys.* **40** 4119
[19] Fursa D V and Bray I 2008 *Phys. Rev. Lett.* **100** 113201
[20] Gangwar R K, Tripathi A N, Sharma L and Srivastava R 2010 *J. Phys. B: At. Mol. Opt. Phys.* **43** 085205
[21] Scheer M, Thøgersen J, Bilodeau R C, Brodie C A, Haugen H K, Andersen H H, Kristensen P and Andersen T 1998 *Phys. Rev. Lett.* **80** 684
[22] Readle J D, Wagner C J, Verdeyen J T, Spinka T M, Carroll D L and Eden J G 2009 *Appl. Phys. Lett.* **94** 251112
[23] Readle J D, Wagner C J, Verdeyen J T, Carroll D L and Eden J G 2009 *Proc. SPIE* **7196** 71960D
[24] Readle J D, Wagner C J, Verdeyen J T, Spinka T M, Carroll D L and Eden J G 2010 *Proc. SPIE* **7581** 75810K
[25] Measures R M 1970 *J. Quant. Spectrosc. Radiat. Transfer* **10** 107
[26] Barmashenko B D, Rosenwaks S and Heaven M C 2013 *Opt. Commun.* **292** 123
[27] Bartschat K 2013 *J. Phys. D: Appl. Phys.* **46** 334004
[28] Zatsarinny O, Wang Y and Bartschat K 2014 *Phys. Rev.* A **89** 022706
[29] Zatsarinny O 2006 *Comput. Phys. Commun.* **174** 273
[30] Zatsarinny O and Bartschat K 2013 *J. Phys. B: At. Mol. Opt. Phys.* **46** 112001
[31] Borovik A, Kupliauskiene A and Zatsarinny O 2011 *J. Phys. B: At. Mol. Opt. Phys.* **44** 145203
[32] Stafford D S and Kushner M J 2004 *J. Appl. Phys.* **96** 2451